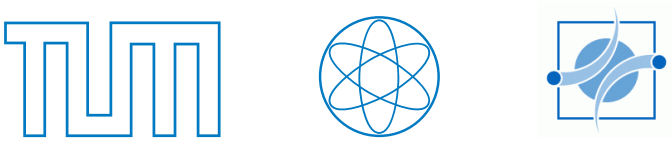

Technische Universität München
Fakultät für Physik
Professur für Experimentalphysik (E12) - Dense and Strange Hadronic Matter

Bachelor thesis in physics

Discharge propagation studies with a single GEM in Ar-CO_2 (90-10)

Untersuchungen zur Entladungspropagation mit einem GEM-basierten Detektor in Ar-CO2 (90-10)

Lautner, Lukas

Garching, October 9th 2017

Supervisor: Dr. Piotr Gasik
Primary Reviewer: Prof. Dr. Laura Fabbietti
Secondary Reviewer:

Primary Reviewer: Prof. Dr. Laura Fabbietti

Secondary Reviewer:

Contents

List of Figures

Chapter 1

Introduction

Gas Electron Multiplier (GEM) [1]-based detectors are widely used in many experiments (COMPASS [2,3], LHCb [4], TOTEM [5,6]) and future upgrades (ALICE [7,8], CMS [9], sPHENIX [10]). Electrical discharges that may occur during operation of those detectors are possibly harmful to hardware and electronics and can damage it permanently in form of increased leakage currents or permanent electric short circuits that render the detector effectively blind. Initial discharges caused by high charge densities compatible with the Raether limit [11] in a single GEM hole [12]. These discharges may propagate through the GEM stack from GEM foil to subsequent GEM foil or from the last GEM to the readout anode. The latter is especially dangerous, as frontend electronics can be severely affected by high energy released in a discharge event. Discharges in GEMs have been extensively studied in [13, 14]. Further studies at TUM and CERN drawn attention to the influence of systematic parameters of the HV scheme have shown that the behavior of the electric field in the gap between GEM foils or GEM foil and anode after an initial discharge can not explain propagated discharges [15, 16]. But in particular the propagated discharge, in opposite to the initial primary discharge, is still not fully understood. Therefore this thesis investigates the mitigation possibilities by systematic study of the RC circuit elements on the secondary discharge probability and develops a basic simulation framework to further the understanding of the phenomenon.

1.1 GEM

A GEM is typically made out of a thin polyimide (e.g. Abical [17]) foil of about 50 µm thickness with a thin (∼5 µm) copper layer applied on bottom and top side. In a photolitographic process holes are etched in a hexagonal pattern from both sides into the foil resulting in a double-conical shape with an inner radius of 50 µm and an outer radius of 70 µm. The standard pitch between holes is 140 µm.

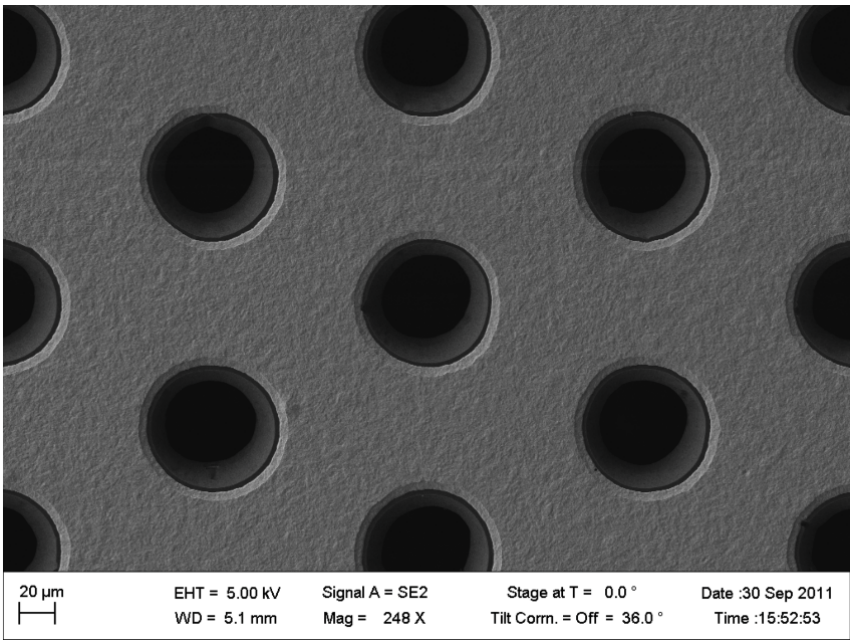

Figure 1.1: Electro microscope image of a standard pitch GEM foil

Voltage is applied to both GEM electrodes resulting in a potential difference ΔU_{GEM} of several hundred volts enabling high fields of about 50 kV/cm inside the holes allowing avalanche multiplication. With a single GEM gains in the order of 10^3 are possible which can be enhanced by subsequently stacking GEMs which also increases operation stability [14]. A simulation of two electrons from the drift region entering the amplification zone is depicted in fig.1.2. In the cross section of a GEM hole it can be seen that the electrons, indicated by yellow lines, get amplified in the high fields of the hole and most of them are extracted. The ions, indicated by red lines, are created in the amplification process and efficiently collected on the top side of the GEM. This showcases the intrinsic ion backflow suppression of a GEM preventing a large fraction of ions to drift back into the drift volume.

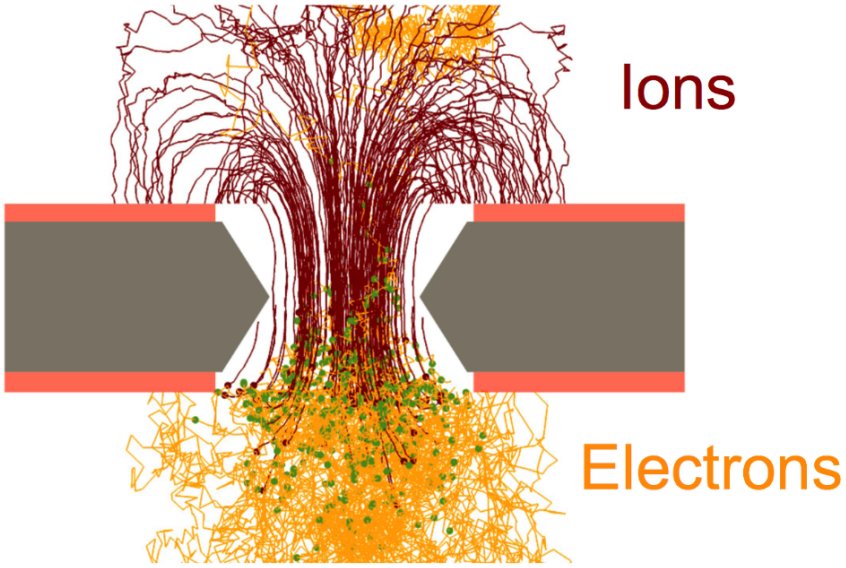

Figure 1.2: Garfield/Magboltz simulation of the amplification process with initially two electrons entering the amplification region. Red lines mark ion, yellow line electron paths. Green dots depict points of ionization.

1.2 Discharges

Discharges pose a threat to the detector system. In general every discharge is a short across two electrodes. In this thesis two types of discharges were observed, the primary discharge occurring between the two GEM electrodes and the propagated discharge between a GEM electrode and the anode. The theory behind primary discharge is understood. A primary discharge is caused by a streamer discharge in a GEM hole after a critical charge in the order of 10^7 electron-ion pairs, compatible with the Raether limit, is reached [12, 13]. The charge locally modifies the electric field and forms a conductive channel the so-called streamer discharge which eventually transforms into a spark, shortening the the upper and lower GEM electrodes.
After a primary discharge a secondary discharge supposedly in the induction gap can occur. This type of discharge is not fully understood. Secondary discharges appear at electric fields that are supposed to be too low to lead to a discharge by established mechanisms [15, 16]. Measurements with HV probes, SPICE and PCB simulations could not find any signs for a significant increase of the electric field anywhere in the system. In addition, between primary and secondary discharges unusual times ($\sim$ µs) are observed which exclude photon-assisted streamer mechanisms. If some photon mechanism would be dominating the secondary discharge should occur faster.

The time between primary and secondary discharges points to field distortion due to space charge-related effects. One hypothesis is that after a primary discharge the extracted charge result in high charge densities in the induction gap which locally increase the electric field enabling a streamer to form which eventually shorts the lower GEM electrode and the readout anode. A collection of hypotheses and possible mechanism can be found in [18].
It seems that secondary discharges can not be avoided but only mitigated. This thesis aims to identify and understand the influence of the power supply on the secondary discharge probability and gives recommendations for a safe and stable operation of a GEM detector. The secondary discharge probability is defined as following:

$$P_{sec} = \frac{N_{sec}}{N_{prim}} \tag{1.1}$$

With N_{sec} being the number of secondary discharges and N_{prim} the number of primary discharges. The statistical error of these quantities follows the Poisson distribution:

$$\Delta N_i = \sqrt{N_i} \tag{1.2}$$

The combined statistical error of the secondary discharge probability is then described by following equation:

$$\Delta P = \sqrt{\frac{N_{sec} \cdot \Delta N_{prim}}{N_{prim}^2} + \left(\frac{\Delta N_{sec}}{N_{prim}}\right)^2} \tag{1.3}$$

Chapter 2

Experimental Setup

2.1 Detector

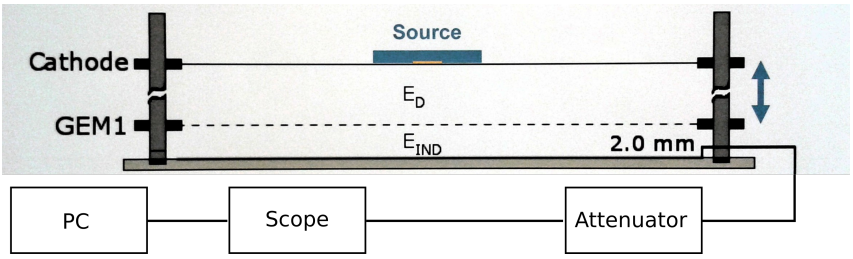

Figure 2.1: Schematic of the detector and readout setup. E_D marks the drift field and E_{ind} the induction field. The padplane is readout via an attenuator by an oscilloscope [19] is connected to a computer.

The detector consists basically of a single GEM (gas electron multiplier) foil with a cathode and a source above and a readout anode below it. All embedded in a metallic box with a removable lid and a gastight gasket in between.
The active area of the padplane measures 10 cm × 10 cm. The anode is fixed with pillars on every corner to a plastic plate isolating the metallic box from the sensitive electronic readout. The GEM foil with its frame is screwed on the anode frame yielding in a distance of 2 mm between anode and GEM. The space between GEM foil and anode is called induction gap, the electric field in this gap is called induction field E_{Ind}. The cathode is placed on a plateau of the pillars with a distance of 19.5 mm to the GEM foil. This gap is called drift gap and the respective electric field in it drift field E_{Drift}. E_{Drift} is constantly held at 400 V/cm for all measurements. For some measurements a cross composed of 1.4 mm wide bars and made out of G11, similar to the material used for the frame, was placed in the induction gap. On top of the cathode a triple alpha source is placed and irradiates the drift volume, see section 2.2 for more details. The detector is constantly flushed with an Argon-CO_2 (90-10) gas mixture, see section 2.3. A field cage was not used.

2.2 Radiation source

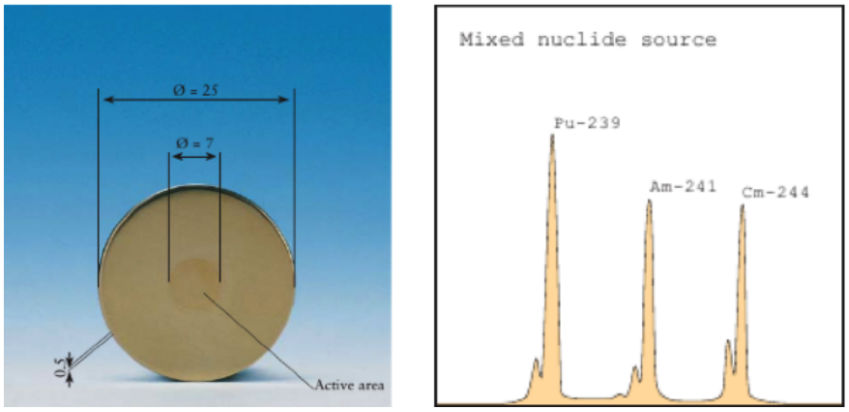

Figure 2.2: The mixed alpha source with its spectrum. [20]

A radioactive source emits ionizing radiation. In case of an alpha source double positively charged $^{4}_{2}$He nuclei are emitted which can travel several centimeters in air before recombining with two electrons to a neutral He atom.
A mixed alpha source containing ^{239}Pu, ^{241}Am and ^{244}Cm is used. The source measures 25 mm in diameter, 0.5 mm in height and the diameter of its active area is 7 mm. The source is placed on a 7 mm hole in the 1.5 mm thick cathode PCB.
A picture of the source and its spectrum can be seen in 2.2. The source emits alpha particles with the weighted energies of 5.155 MeV for ^{239}Pu, 5.486 MeV for ^{241}Am and 5.805 MeV for ^{244}Cm. [20] The alpha rate measured by the detector is 550 Hz.

2.3 Gas

For all measurements the detector is flushed with a Ar-CO_2 (90-10) gas mixture keeping a constant flow of 10 L/h. A slight overpressure of few mbar is maintained in the detector. Through the amplification processes excited and ionized noble gas atoms are produced. These can cause further avalanches which can lead to discharges. To counter this and terminate discharges before they occur a quencher gas is introduced. Excited atoms deexcite via radiative transitions emitting UV photons which then can create free charges on metallic surfaces in the detector through the photoelectric effect which could potentially lead to new avalanches in different locations. Ions on the other hand drift to the cathode and can neutralize there by extracting an electron and emitting UV photons or extracting a second electron due to energy conservation. Thus also increasing the risk of additional avalanches and discharges.

To avoid discharges caused by above processes CO_2 as a quencher is added which has a lower ionization potential than the noble gas and can therefore easily exchange charge with the noble gas ions. Although the molecule ions also neutralize at the cathode they get rid of their excess energy by dissociating. As the quencher gas is a molecule it can also absorb UV photons created by the amplification processes through its vibrational and rotational states.
Argon is a noble gas and as such is characterized through its filled subshells which makes it chemically inert with a high ionization energy. In a gas mixture charged particles which travel through it scatter inelastically with its constituents and ionize the atoms and molecules. The energy needed to create on average an electron-ion pair taking in account all viable processes is called the effective ionization potential W_i. In the course of this thesis Argon-CO_2 (90-10) was exclusively used. The respective effective ionization potential amounts to 28.19 eV. A contamination with electronegative gases like O_2 or H_2O leads to an attachment of low energy electrons to these gases which would reduce the detected charge greatly. Therefore the oxygen and water contamination is monitored and it is made sure to keep the oxygen level below 20 ppm and the water contamination in the ppm region.
For monitoring the gas flow, oxygen concentration, water concentration and (over)pressure a Cambridge Sensotec rapidox3100 [21] was used.

2.4 Readout scheme

The readout anode is connected to an adjustable attenuator damping the signal by up to 34 dB. This is needed to get a signal with a low enough signal amplitude which can be measured. The outgoing signal from the attenuator is feeded into the scope that records the data and transfers the waveforms after the run to the computer where they will be saved and can be accessed via the Xviewer software [22].

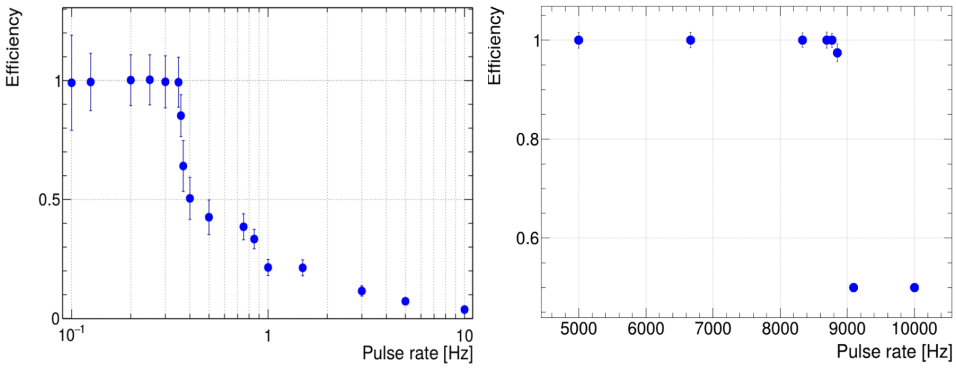

Figure 2.3: Comparison of the saving efficiency as a function of the pulse rate of the old and new scope. On the left one can see that the old scope lacks high rate capability with the saving efficiency dropping at a pulse rate of about 0.3 Hz. The right plot shows that the new scope now enables saving of high rate measurements up to a pulse rate of circa 9000 Hz

The typical signal amplitude caused by an alpha particle is in the order of a few mV whereas a discharge signal has an amplitude of (several) Volts. The time difference between primary and secondary discharge signal varies with the setting between some ns and several µs. The duration of the discharge signals fluctuate between several ten to hundreds of ns. With discharge rates of about 1 Hz to record all events a readout frequency of at least 1 Hz is required. The saving efficiency of the oscilloscope used for previous studies dropped rapidly at a pulse rate of around 0.3 Hz which in addition can not be directly connected to a computer and has only very limited memory space available. So that the data would have been to be recorded an analog setup which would lead to a problem as with changing settings also the signal form changed which makes this method impractical. Therefore a new oscilloscope has been acquired enabling a efficient readout even with a pulse rate of several thousand Hertz. Thus we can abandon NIM-logic readout based on the discriminators, gate generators and scalers.
Compared with the saving efficiency of the old scope which dropped at a pulse rate of around 0.3 Hz the new Yokagawa DLM 2054 [19] scope comes with a notable higher saving efficiency for high rates, dropping only at roughly 9000 Hz and therefore enables saving measurements with reasonable high data rates 2.3.

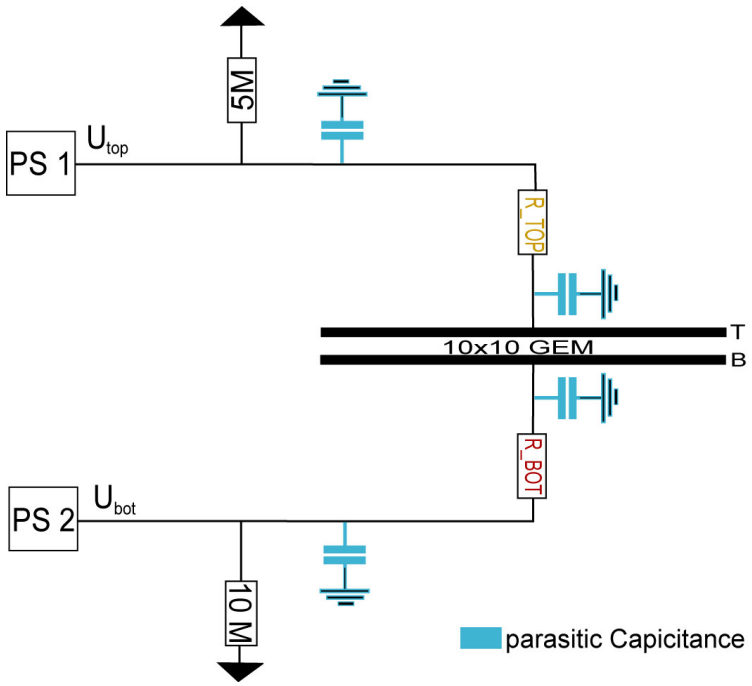

Figure 2.4: Overview of the experimental HV setup. Marked in blue are the parasitic capacitances of the cables between components. Those parasitic capacitances are variable via changing the cable length of the respective cable. R_{top} between GEM top (T) and a 5 MΩ decoupling resistor and R_{bot} between GEM bottom (B) and a 10 MΩ decoupling resistor are also variable. PS1 for GEM top and PS2 for GEM bottom denote the independent channels of the power supply.

The principle schematic of the high voltage setup used in the measurements is depicted in 2.4. The potentials of both GEM electrodes are provided by separate channels of a iseg EHS F 060nILK [23] HV power supply.
A 10 MΩ resistor to ground is connected in series to GEM bottom, likewise a 5 MΩ resistor to ground is connected to GEM top. Through those resistors to ground a constant current is ensured. That means in case of a HV trip the current limit of the power supply will be exceeded and it shuts down, which guarantees a safe discharge of the GEM foils. Decoupling resistors R_{bot} and R_{top} are connected in series to the respective GEM electrodes. As depicted in 2.4 there are cables connecting GEM electrodes and decoupling resistors and decoupling resistors and resistors to ground. These are considered parasitic capacitances and are as well as the decoupling resistors varied to study their influence on the secondary discharge behavior of the system.

2.5 Properties and types of signals

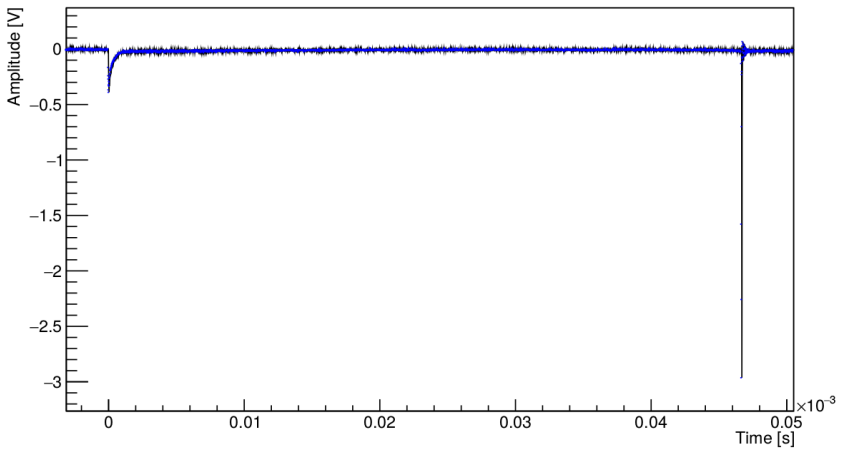

Figure 2.5: A typical signal with a primary discharge followed by a secondary discharge. The time difference is measured peak to peak. Note that it lies in the order of µs. E_{ind} is here 6700 kV/cm and R_{bot} is set to 100 kΩ

There are two types of discharges which are distinguish by their signal shape and associated origin. The primary discharge is associated with a spark in a GEM hole after a certain critical charge Q_{crit} in it is reached, effectively shorting the upper and lower GEM electrode. It is characterized by a initial peak with negative amplitude and following rapid oscillations defined by RLC elements of the circuit. The probability for a primary discharge increases with the applied voltage difference between GEM top and bottom side ΔU_{GEM} and induction field E_{ind}. For configurations for which there are constant primary discharges the increase of E_{ind} gives rise to secondary discharges. These kind of discharges occur way below the breakdown field in the induction gap which raises questions over the underlying physical processes.
A secondary discharge is in general always preceded by a primary discharge. For high E_{ind} it is possible that a primary is followed by more than one secondary discharge. There exist exceptions at very high induction fields of way over 10 kV/cm in Ar-CO_2 (90-10) where secondary discharge like signals can be observed without previous primary discharge. This can be seen as further prove that secondary discharges are discharges in the induction gap and are caused by space charge-like effects. See also 3.1.1.
The secondary discharge probability rises sharply from its onset to the point where every primary is followed by a secondary discharge. The origin of the secondary discharge is supposedly allocated in the induction gap and in opposition to the primary discharge the initial negative peak is not followed by oscillations.

Fitting the association of charge extraction from a GEM hole after a primary discharge with the origin of secondary discharges in the induction gap an increase of E_{ind} and thus the enhancement of the extraction rate results likewise in a rise of the amplitude of the secondary discharge signals. Besides the amplitude and probability also the time difference between primary and secondary discharge ΔT is varying between settings dependent on resistance, capacitance and E_{ind}. But a common denominator is that ΔT is inverse proportional to E_{ind} as with higher E_{ind} more energy is deposited in the induction gap and thus the recharging time after a discharge is shorter.
For lower E_{ind} the amplitude of a primary discharge is larger than that of a secondary discharge. This does not hold true for higher E_{ind} as the reverse is observed. This can be again explained by the influence of the induction field on the charge extraction from the GEM to the induction gap. As ΔU_{GEM} is not changed and the extraction to the induction gap is increased with E_{ind} the amplitude of a primary discharge can not grow larger and even decreases with increasing E_{ind}. The contrary can be seen for secondary discharges as their amplitude grows larger with more charges extracted to the gap.
In the course of this thesis some experimental issues were encountered.
Those where mostly related with induction fields of around 8 kV/cm and higher.
One issue is that not only the amplitude but also the signal shape changes with higher E_{ind} and different RC settings. The higher the electric field the more pronounced is the initial peak in the signal. This can be explained by the increase of the extraction efficiency with higher induction field which leads to more charges moving into the induction gap and thus inducing a different signal shape on the padplane. This makes an automatic processing of the obtained data nearly impossible as no reliable signal pattern can be found.
A different problem is encountered at higher E_{ind} where ΔT drops so that primary and secondary discharge signals are no longer dependably to distinguish as they appear fused together. For cases where it is not clear if just a primary or a primary and a secondary discharge was observed a single primary discharge was assumed. Configurations with this problem are marked accordingly in plots and discussions.
Another experimental issue regarding a completely new type of signal was resolved after intensive studies. As in the course of these studies the induction fields were subsequently increased ($E_{ind} > 9$ kV/cm) irregularities were noticed at the end of the used 100 µs time window. After extension of the time window to 500 µs these irregularities were proven to be strange signals characterized by unusual large peak and oscillation amplitudes. A defining trait of this signal is the sharp onset of the negative peak and its oscillation as seen in fig.3.7 which is dominated by a very high first positive peak and gets rapidly dampened. In its signal shape those signals resemble secondary discharges.
These signals appear with and with out prior secondary discharges and at very high

induction fields and are created in the induction gap as if the potential ΔU_{GEM} is set to zero these kind of signals can be still observed. Therefore there is no association with primary discharges. Measurements with a cross in the induction gap to prevent bending of the GEM foil due to gravity as discussed in sec.3.1.1 indicate that these new signals are caused by a sagging GEM foil which at a very high E_{ind} create high enough fields which are enough for a discharge even without a primary spark. These signals are identified as discharges in the gap and were not taken into account during analysis.

Chapter 3

Results

3.1 Experimental results

3.1.1 Measurements with cross

To create a spark discharge between two electrodes a sufficiently high electric field is needed. But the measurements in this thesis show that discharges are observed well below the breakdown and even amplification field. Therefore the field has to be increased by a streamer creation mechanism or trivial hardware-related effects.
One possible explanation could be that the GEM foil bends due to gravity towards the readout anode and thus creates a high enough electric field for discharges to occur by the streamer mechanism. To study this explanatory approach a cross with equal-length, orthogonal arms made from G11 which is similar to the FR4 material used for the frame was placed inside the detector between GEM foil and anode to prevent sagging of the foil.

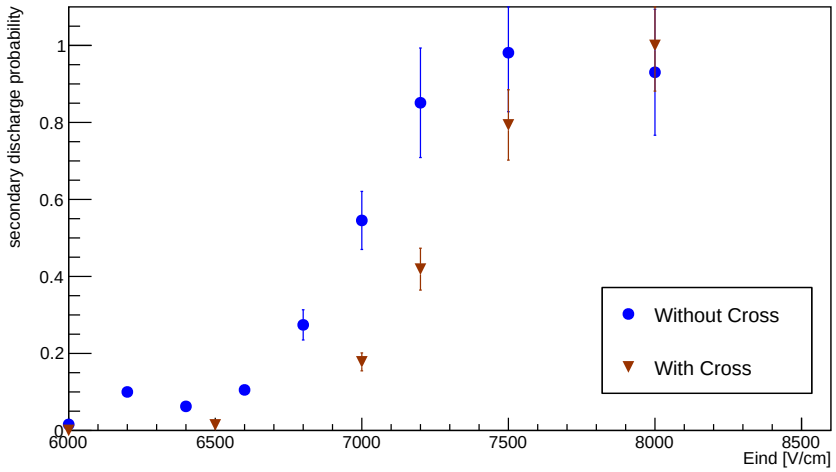

Figure 3.1: Measurements with and without cross in the induction gap. With R_{bot} set to 200 kΩ and R_{top} to 10 MΩ.

If the potential difference between both GEM electrodes ΔU_{GEM} is set to zero naturally no primary discharges appear. However if additionally a very high E_{ind} (above 10 kV/cm) is applied secondary discharges can still be observed. This gives a lower limit to E_{ind} to have secondary discharges in the induction gap without prior primary discharges which is still below amplification and breakdown field strengths.
The measurements with and without cross for moderate induction fields show that with a cross leads to a slightly later onset of secondary discharges but no significant difference3.1.
Thus bending of the GEM foil delivers no explanation for secondary discharges at low to moderate E_{ind}. Additional to the foil bending the charging-up effect of frame material in the induction gap can be studied through this measurement as the cross is made from a similar non-conducting material as the frame. So as well as the foil bending the collection of charge on the surface of the cross has no significant influence on the secondary discharge probability at moderate to high values of E_{ind}.
Other possibilities concern the HV supply response which is studied in the following sections as parameters of the electrical circuit are systematically examined and physical space-charge effects for which a simulation framework has been developed.

3.1.2 RC scan of the system

3.1.2.1 Capacitance at GEM top

Two configuration were used for the placement of R_{top}. Cables connect the power supply to the 5 MΩ resistor to ground and the resistor to ground to the decoupling resistor R_{top} 2.4. From there the configurations differ. One variant is outside of the detector with a short cable from the upper GEM electrode to the detector wall and from there via a short SHV cable to a box with the decoupling resistor soldered inside. For the other configuration R_{top} is directly soldered on the flap of the GEM upper side inside of the detector. The inside variant has a negligible parasitic capacitance to ground in comparison to the outside variant where the extra cables imply also an extra capacitance.

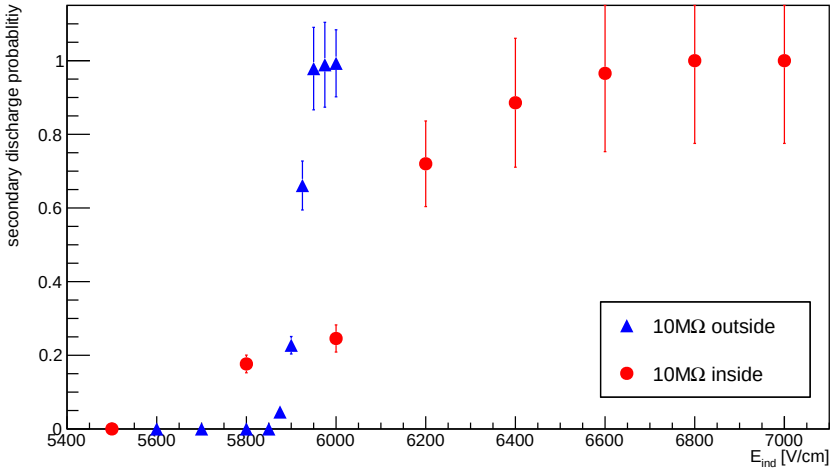

Figure 3.2: R_{top} placement inside and outside of detector

The secondary propagation probability is plotted against the induction field for the two configurations in fig.3.2. For both variants R_{bot} is set to 100 kΩ and R_{top} to 10 MΩ. The higher parasitic capacitance of the outside configuration shifts the propagation curve towards lower E_{ind}. This can be seen as a result of the additional energy stored in the cables which puts extra charge in the system leading to a full propagation probability at relatively low induction fields. For the inside variant this additional energy is not available therefore it needs a higher E_{ind} to reach the same secondary discharge probability to compensate for this.
For that reason it is clearly recommended to minimize the (parasitic) capacitance between the upper GEM electrode and its respective decoupling resistor R_{top}. In

this thesis the inside configuration with R_{top} directly connected to the GEM upper side is used for all measurements.

3.1.2.2 Resistance at GEM top

The decoupling resistor R_{top} is located on the upper side of the GEM (cf. fig.2.4). In case of a primary discharge a high resistance on the GEM top should decrease U_{top} and therefore increases E_{drift}. Which is used to quench primary discharges as the potential difference between lower and upper electrode is diminished.

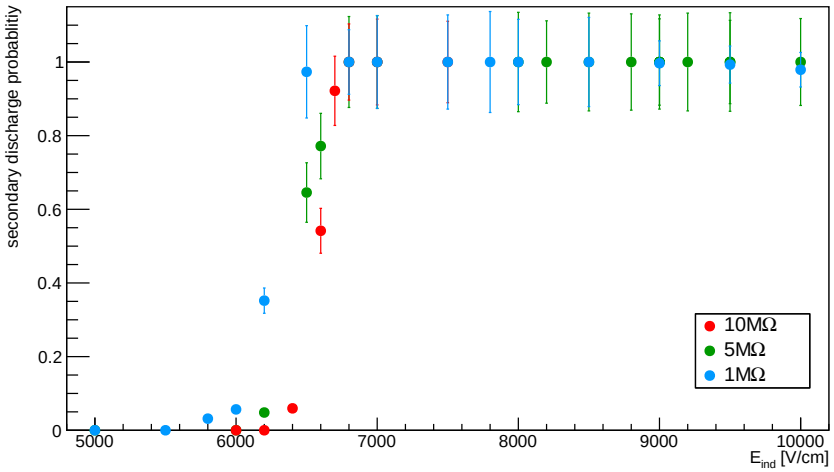

Figure 3.3: Secondary discharge probability for different R_{top}

The secondary discharge probability is plotted as function of R_{top} for 100 kΩ at GEM bottom in fig.3.3. Obviously there is no significant influence of R_{top} over a wide range of values for the decoupling resistor.

3.1.2.3 Resistance at GEM bottom

A parameter of great interest is the decoupling resistor R_{bot} at GEM bottom. A large R_{bot} should increase the potential U_{bot} of the lower GEM electrode after a primary discharge. With an increase of U_{bot} an increase of E_{ind} is accompanied. Therefore the secondary propagation should start earlier for bigger values of R_{bot}.

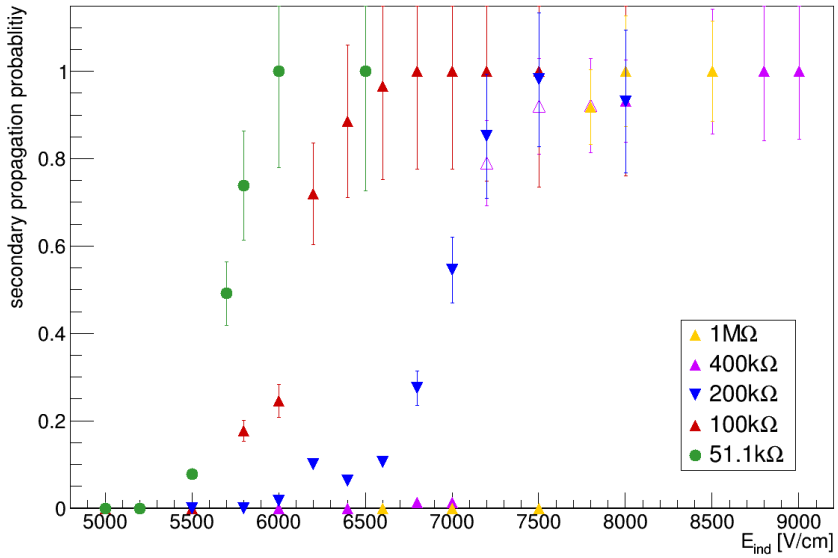

Figure 3.4: Secondary probability as function of E_{ind} for different values of R_{bot} and R_{top} set to 5 MΩ . Hollow points mark configurations were it is difficult to distinguish primary discharges from primary discharges that already fuse with secondary discharges

The measurements3.4 give a contrary picture. For a larger resistance at GEM bottom the start of secondary propagation is shifted to higher induction fields. This was not expected and can not be explained at the moment.

3.1.2.4 Capacitance at GEM bottom

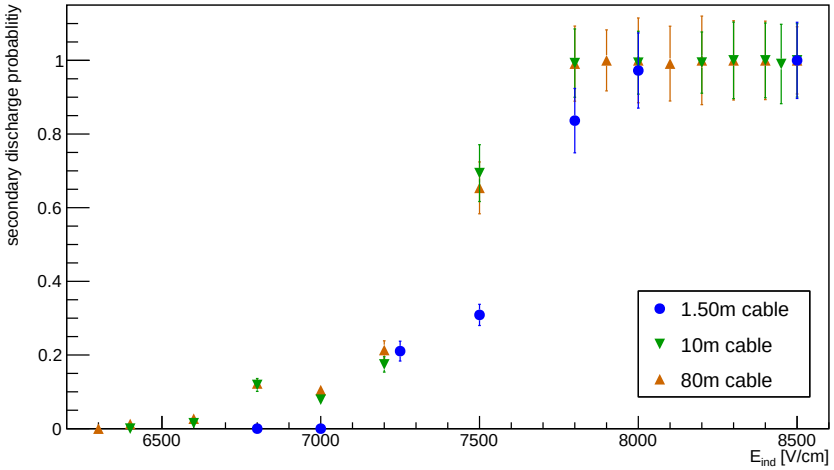

Figure 3.5: Different cable lengths after R_{bot} at GEM bottom.

The coaxial cable between decoupling resistor R_{bot} and the 10 MΩ loading resistor to ground in the standard configuration used for every other measurement is 1.50 m long which corresponds to a 150 pF capacity. In this study this cable was replaced with a 10 m and a 80 m cable respectively a 1 nF capacity and a 8 nF capacity. 100 pF/m is a typical capacity per length for these kind of cables thus the values in this thesis are derived from it. For all of these measurements the R_{bot} was 200 kΩ. In fig.3.5 the secondary propagation probability for the different configurations is plotted against the induction field. As expected the additional resistor R_{bot} decouples the system and makes sure that the extra capacity has no influence on the system. Therefore the use of a decoupling resistor for the GEM powering scheme can be clearly recommended. The point where the value of R_{bot} is too low to decouple the system is an interesting aspect that will be studied in the future.

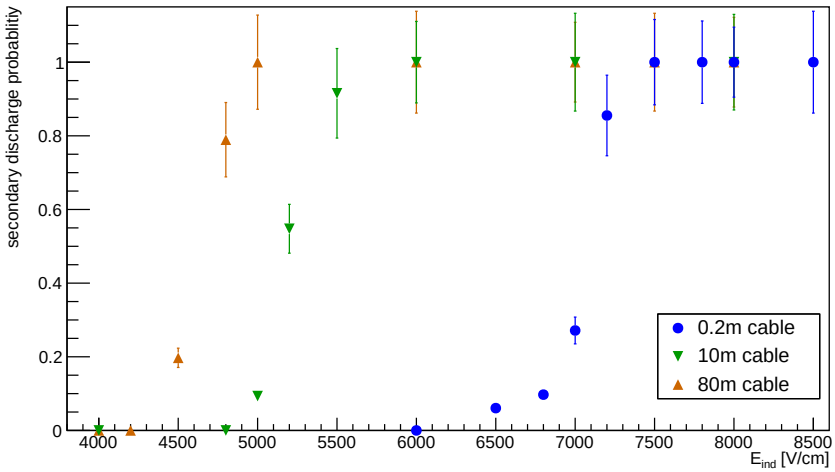

Figure 3.6: Different cable lengths between R_{bot} and GEM bottom

The cable between the lower GEM electrode and the decoupling resistor R_{bot} is in standard configuration 0.2 m long corresponding to a parasitic capacitance of 20 pF. To study the influence of this capacitance the cable length and thus the parasitic capacitance between the lower GEM electrode and R_{bot} got varied2.4. In addition, measurements with 10 m and 80 m cables were conducted.
In fig.3.6 it becomes apparent that with higher capacitance the secondary propagation starts at lower induction fields. This can be explained thereby that with higher capacitance more energy gets stored in the system which may keeps the effective E_{ind} after a primary discharge higher and thus favors a secondary.
Thus to increase the safety of GEM detector systems and inhibit secondary discharges it can be recommended to reduce the capacitance between the GEM bottom and R_{bot}. This can be done by keeping the cables short or even soldering the decoupling resistor directly to the lower GEM electrode.

3.1.2.5 Experimental issues

In the course of this thesis some experimental issues related to measurements with induction fields of around 8 kV/cm and higher were encountered.
One issue is that not only the amplitude but also the signal shape changes with higher E_{ind} and different RC settings. Higher the electric field the more pronounced is the initial peak in the signal. This can be explained by the increase of the extraction efficiency with higher induction field which leads to more charges moving in the induction gap and thus inducing a different signal shape on the padplane. This makes an automatic processing of the obtained data nearly impossible as no

reliable signal pattern can be found.
A different problem is encountered at higher E_{ind} where ΔT drops so that primary and secondary discharge signals are no longer dependably to distinguish as they appear fused together. For cases where it is not clear if just a primary or a primary and a secondary discharge was observed a single primary discharge was assumed. Configurations with this problem are marked accordingly in plots and discussions.

Figure 3.7: Closeup of a discharge signal induced by foil bending in the induction gap at an induction field of 11 kV/cm. The x axis displays the time divided into 100 ns divisions respectively the y axis displays the amplitude in 1.5 V divisions.

3.2 Simulation framework for a space charge induced diffusion-assisted streamer in the induction gap

The experimental results hint to a space charge related mechanism for secondary discharge creation. To accompany the experimental results a COMSOL simulation has been developed. COMSOL is a multiphysics simulation software solving problems

with finite element methods. The version used for the simulations in this thesis was COMSOL Multiphysics 5.2 [24].
The simulation is based on a hydrodynamic model for streamer development in a single GEM hole by P. Fonte [25] and work by F. Resnati et al. [26]. As observed in the experiments the time between primary and propagated discharge is too short to be caused by drifting charges which would bombard GEM electrodes liberating electrons causing a secondary emission and too long to be caused purely by photons. Therefore a space charge effect seems to be the most plausible explanation. The idea behind the simulation is to prove that such a space charge induced diffusion-assisted streamer can develop in the induction gap in accordance with observations. The induction gap on the upper side delimited by the GEM and on the underside by the readout anode.This basically constitutes a plate condensator with the lower GEM electrode as cathode and the padplane as anode. This was recreated in COMSOL in a 2D axisymmetric geometry with a radius of 0.5 mm and 1 mm distance between anode and GEM foil. The down scaling to a smaller geometry than the one used in the measurements intends to achieve reasonable simulation runtimes while still obtaining a decent resolution. The simulation times are rather short with a maximum of 100 ns which makes it reasonable to neglect the movement of positive ions. Photonic effects are considered with according parameters represented by effective values, averaged over all wavelengths.
Beginning with an initial charge cloud in a half spheroidal volume under the cathode simulating the charge emitted under a GEM hole, the electrons are then accelerated by an electric field towards the anode and subjected to the space charge ρ.

$$\rho = q \cdot (n_{ions} - n_{electrons}) + \rho_0 \tag{3.1}$$

The space charge is composed of the difference of positive and negative charges and a constant addend ρ_0 which is introduced to denote a pre-existing space charge 3.1. The simulation terminates when the streamer reaches the cathode or when the simulation time is exceeded. For $\rho_0 = 0.02\,\mathrm{C/m^3}$ the formation of a streamer in CO_2 can be seen in **??**. For the initially applied electric field below the breakdown field of the gas mixture a certain critical value of ρ_0 should enable a streamer discharge. In pure CO_2 a streamer will not develop for ρ_0 below $0.008\,\mathrm{C/m^3}$ which corresponds to $4.03 \cdot 10^8$ electrons equally distributed in the whole gap. This would translate to $4.49 \cdot 10^4$ electrons in a GEM hole volume which is 2 order of magnitudes lower than the critical charge for discharges in a GEM hole [12]. It is also compatible with the Raether limit of 10^6-10^7 electrons and as it is spread out in the volume in opposite to the Raether limit which assumes a more or less condensed charge cloud the simple assumption of a constant space-charge ρ_0 seems to be reasonable and yields realistic results. The current version delivers a basic simulation framework which already achieves reasonable results in CO_2. For future studies a more experiment orientated configuration using Ar-CO_2 and an adapted geometry will be developed.

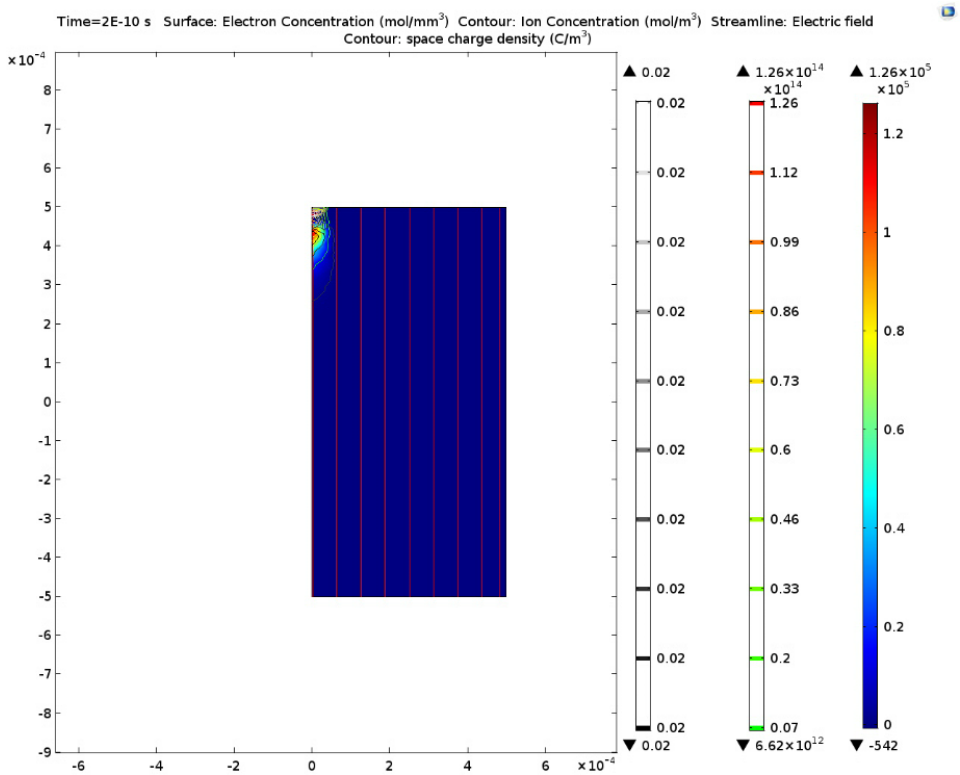

Figure 3.8: The formation of a streamer in the induction gap for $rho_0 = 0.02\,\mathrm{C/m^3}$.The surface colors depict the electron density. The red streamlines the electric field, the contour in grey and black the space charge densities and the colored contour the ion density. Start of simulation. A charge cloud moves from the cathode towards the anode

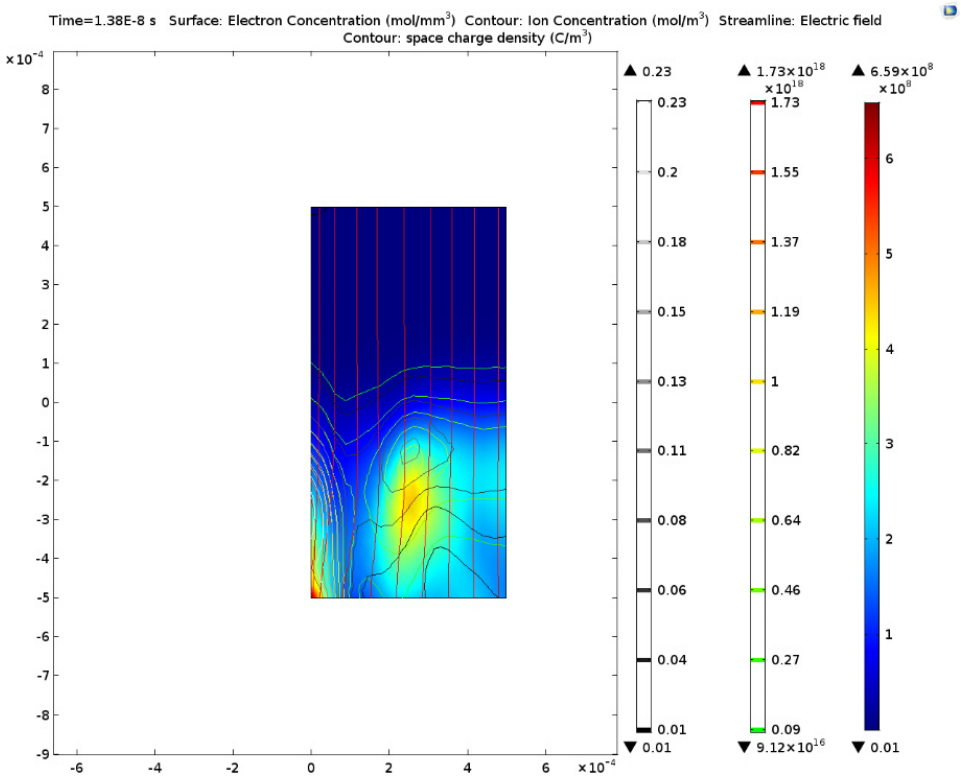

Figure 3.9: A streamer starts to form as the space charge density increased due to self-photoionization of the gas

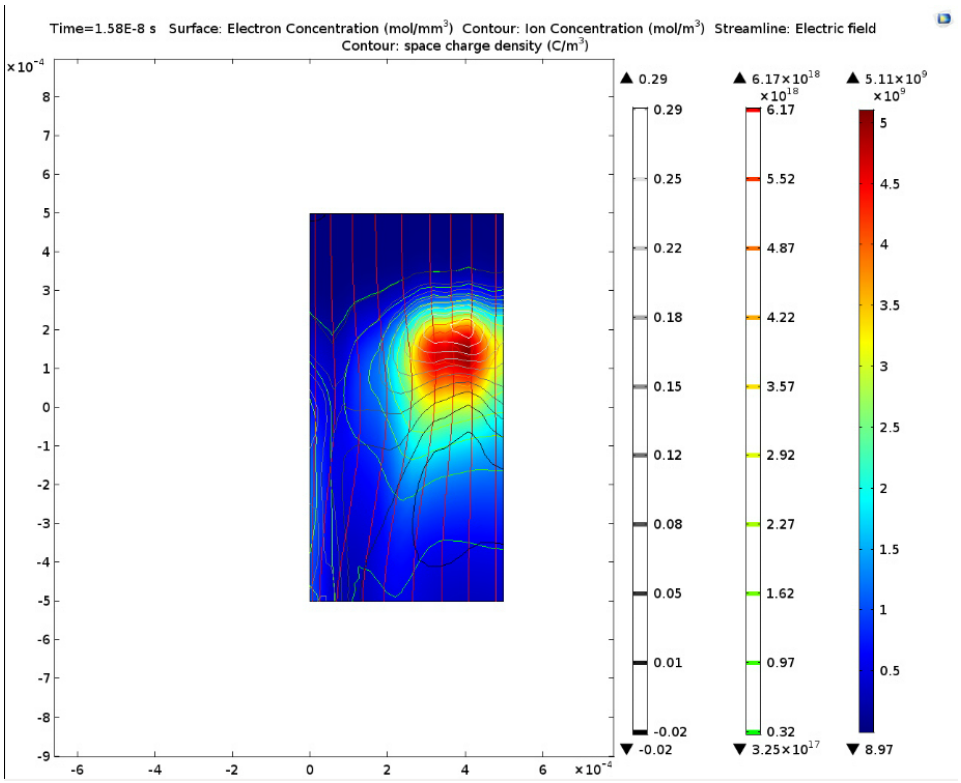

Figure 3.10: Streamer shortly before reaching the cathode and shorting the induction gap

Chapter 4

Outlook

This thesis opens up new questions that require a continuation of studies to fully understand the nature and origin of secondary discharges. The inductivity of the system has yet not been considered but self-evidently has some influence on the system. As shown in this thesis while it is not possible to completely avoid secondary discharge it is possible to mitigate them by the right choice of electrical components such as cables and decoupling resistors. As the physics is still not understood but all evidence pointing in the direction of a space charge related effect the basic simulation framework established in this thesis has to be build up on and set to use on realistic gas mixtures to gain insight into the underlying physics. Although difficult to as the the discharge signal is heavily influenced by the RC components and fields signal shape analysis could answer some questions.

4.1 Development of new transparent detector

In the course of this thesis a new model for future detectors was developed in Solidworks and is currently build.The new detector model features transparent elements on five sides allowing for optical readout. Furthermore the new design significantly improves the tightness and will be able to suppress the oxygen contamination from now 10 ppm at best down to sub-ppm levels enabling distortion-free signal measurements. Future plans intend to use this detector with a CCD or CMOS high-speed camera to optically observe and analyze secondary discharges in the induction gap.

Bibliography

[1] F. Sauli. GEM: A new concept for electron amplification in gas detectors. *Nucl.Instrum.Meth. A* (1977).

[2] C. Altunbas. Construction, test and commissioning of the triple-gem tracking detector for compass. *Nucl.Instrum.Meth. A* **490** (2002).

[3] B. Ketzer. Micropattern gaseous detectors in the COMPASS tracker. *Nucl.Instrum.Meth. A* **494** (2002).

[4] G. Bencivenni, G. Felici, F. Murtas, P. Valente, W. Bonivento, A. Cardini, A. Lai, D. Pinci, B. Saitta & C. Bosio. A triple-GEM detector with pad readout for high rate charged particle triggering. *Nucl.Instrum.Meth. A* **488** (2002).

[5] M. Bozzo, M. Oriunno, L. Ropelewski, F. Sauli, R. Orava, J. Ojala, K. Kurvinen, R. Lauhakangas, J. Heino, W. Snoeys, F. Ferro, M. Van Stenis & E. David. Design and construction of the triple GEM detector for TOTEM. In *Nuclear Science Symposium Conference Record, IEEE (2004)* 447 – 450 Vol. 1 (2002).

[6] M. G. Bagliesi, M. Berretti, E. Brücken, R. Cecchi, E. David, F. García, V. Greco, J. Heino, T. Hilden, K. Kurvinen, R. Lauhakangas, S. Lami, G. Latino, G. Magazzù, E. Oliveri, E. Pedreschi, L. Ropelewski, A. Scribano, F. Spinella & M. Van Stenis. The TOTEM T2 telescope based on triple-GEM chambers. *Nuclear Instruments and Methods in Physics Research Section A: Accelerators, Spectrometers, Detectors and Associated Equipment* **617**, 134–137 (2010).

[7] B. Ketzer. A time projection chamber for high-rate experiments: Towards an upgrade of the ALICE TPC. *Nuclear Instruments and Methods in Physics Research A* **732**, 237–240 (2013).

[8] C. Lippmann. A continuous read-out TPC for the ALICE upgrade. *Nuclear Instruments and Methods in Physics Research Section A Accelerators Spectrometers Detectors and Associated Equipment* **824**, 543–547 (2016).

[9] A. Colaleo, A. Safonov, A. Sharma & M. Tytgat. CMS Technical Design Report for the Muon Endcap GEM Upgrade. Tech. Rep., CERN (2015).

[10] C. Aidala, N. N. Ajitanand, Y. Akiba, R. Akimoto, J. Alexander, K. Aoki, N. Apadula, H. Asano, E. T. Atomssa, T. Awes, B. Azmoun, V. Babintsev, M. Bai, X. Bai, N. Bandara, B. Bannier, K. N. Barish, O. Baron, B. Bassalleck & C. Zumberge. An Upgrade Concept from the PHENIX Collaboration. *Nuclear Physics A* (2012).

[11] H. Raether. *Electron avalanches and breakdown in gases*. Butterworths advanced physics series (Butterworths, London, 1964). URL `https://cds.cern.ch/record/102989`.

[12] P. Gasik, A. Mathis, L. Fabbietti & J. Margutti. Charge density as a driving factor of discharge formation in GEM-based detectors. *Nucl.Instrum.Meth. A* **870**, 116–122 (2017).

[13] e. Bressan. High rate behavior and discharge limits in micro-pattern detectors. *Nucl.Instrum.Meth. A* **424** (1999).

[14] S. Bachmann, A. Bressan, M. Capeáns, M. Deutel, S. Kappler, B. Ketzer, A. Polouektov, L. Ropelewski, F. Sauli, E. Schulte, L. Shekhtman & A. Sokolov. Discharge studies and prevention in the gas electron multiplier (GEM). *Nuclear Instruments and Methods in Physics Research Section A: Accelerators, Spectrometers, Detectors and Associated Equipment* **479**, 294–308 (2002).

[15] A. Deisting & C. Garabatos. Discharge and stability studies for the new readout chambers of the upgraded ALICE TPC. *Journal of Instrumentation* **12**, C05017 (2017). URL `http://stacks.iop.org/1748-0221/12/i=05/a=C05017`.

[16] P. Gasik. Discharge Studies with Single- and Multi-GEM Structures in a Scope of the ALICE TPC Upgrade. URL `https://indico.cern.ch/event/496113/contributions/2008281/attachments/1242032/1827187/gasik_11032016_sparks_RD51.pdf`. Talk during the RD51 Collaboration meeting (March 2016).

[17] URL `https://www.kaneka.com/kaneka-americas/products/apical`.

[18] V. Peskov & P. Fonte. Research on discharges in micropattern and small gap gaseous detectors. *ArXiv e-prints* (2009). `arXiv:0911.0463`.

[19] Yokogawa Meters & Instruments Corporation. *DLM2000 Series Digital Oscilloscope/Mixed Signal Oscilloscope User's Manual*, 9 edn. (2016). URL `https://www.yokogawa.com/pdf/provide/E/GW/IM/0000022837/0/IM710105-02E.pdf`.

[20] E. . Ziegler. *Alpha spectrometry sources*. URL http://www.ezag.com/fileadmin/ezag/user-uploads/isotopes/isotopes/Isotrak/isotrak-pdf/Product_literature/EZN/04_section04_alpha_spectrometry_sources.pdf.

[21] Cambridge Sensotec Ltd. *Rapidox 3100 Gas Analyser*.

[22] Yokogawa Meters & Instruments Corporation. *701992 Xviewer User's Manual*, 20 edn. (2017). URL https://www.yokogawa.com/pdf/provide/E/GW/IM/0000018845/0/IM701992-01E.pdf.

[23] *iseg*. URL http://www.iseg-hv.com.

[24] URL https://www.comsol.com.

[25] P. Fonte. Calculation of streamer development in MPGDs in an axisymmetric hydrodynamic model. URL https://indico.cern.ch/event/89325/contributions/2108964/attachments/1089488/1554083/Calculation_of_streamer_development.pdf (2010).

[26] S. Franchino, D. Gonzalez Diaz, R. Hall-Wilton, H. Muller, E. Oliveri, D. Pfeiffer, F. Resnati, L. Ropelewski, M. Van Stenis, C. Streli, P. Thuiner & R. Veenhof. Effects of High Charge Densities in Multi-GEM Detectors (2015).

Acknowledgements

I would like to thank everyone who helped and supported me throughout this thesis and prior studies. First of all, professor Laura Fabbietti who gave me the opportunity to work and learn in her motivated group. Furthermore my supervisor Piotr Gasik. Thank you for all your guidance, patience and support! I also would like to thank Andreas Mathis and Thomas Klemenz as they taught me a lot especially in the laboratory and were a great help whenever i had questions. Bernhard Hohlweger is to be thanked for his steady cheerfulness. I want to thank E18 for sharing their laboratory and clean room with us. I also want to thank Ralf Lang and the E12 workshop for their irredeemable help with building the transparent detector. The whole E12 group also deserves a big thank you for making the workplace more than just a workplace. Finally i want to thank my mother and grandmother for the consideration and support.